

Peculiar-velocity distribution functions and 21-cm fluctuations

Ryan Yuran Zhang and Marc Kamionkowski

*William H. Miller III Department of Physics and Astronomy,
Johns Hopkins University, 3400 N. Charles Street, Baltimore, MD 21218, U.S.A.*

(Dated: May 18, 2026)

Predictions for observables involving the cosmological 21-cm background require calculations of spatial correlations of star formation rate densities (SFRDs) which have a nonlinear dependence on the baryon-dark matter relative velocity. Prior work derived these SFRD correlations with a simplifying assumption that neglected the difference between the correlations of the components of the velocity parallel and perpendicular to the separation between the two points being correlated. Here we calculate the full joint PDF of the squares of the peculiar velocity at two different points. The error that arises in predictions for 21-cm fluctuations if this subtlety is overlooked is generally less than a few percent, but it can be larger for some values of wavenumber k and redshift z if there are cancellations between different contributions to the total signal. The correct expression is easily implemented and increases the run time of the code by only a few percent.

I. INTRODUCTION

As the statistics in galaxy surveys and cosmic microwave background (CMB) maps improve, correlation functions that are higher order in cosmological perturbations begin to become accessible. Among the many possible such correlations, there are now several being studied that involve the square of the peculiar-velocity field. For example, 21-cm intensity fluctuations may exhibit velocity acoustic oscillations (VAOs) [1, 2] that arise from correlations between observables proportional to the square of the peculiar velocity field. Similarly, observables proportional to the velocity squared have been suggested for kinematic Sunyaev-Zeldovich (kSZ) tomography [3–5].

In linear perturbation theory, the peculiar velocity is obtained from the gradient of the density field which is itself a realization of a Gaussian random field. Each of the three components v_i (for $i = x, y, z$) of the peculiar velocity is thus a Gaussian random variable, and the one-point probability distribution function (PDF) of $\mathbf{v}^2 = v_x^2 + v_y^2 + v_z^2$, the magnitude squared, is thus a χ_n^2 distributed variable with $n = 3$ degrees of freedom (the Maxwell-Boltzmann distribution). It is then natural to surmise that the joint PDF for the values of \mathbf{v}^2 at two different points is that for two correlated χ_n^2 degrees of freedom, related to the Wishart distribution, as shown, for example, in the Appendix of Ref. [6] (see also Refs. [7, 8]). This assumption was made in Ref. [9] (and implemented in Zeus21¹) to obtain correlation functions for star formation rate densities (SFRDs), which depend nonlinearly on the square of the peculiar velocity.

However, the joint PDF for the values of \mathbf{v}^2 at two different points is not strictly speaking described in this way, as the correlations of the components of the velocity aligned with the separation of the two points being correlated differ from those for the components transverse to that separation. Here we explain and quantify this

subtlety and explore its implications for calculations of 21-cm observables. Although the impact on observables is relatively small for most wavenumbers and redshifts, it can be larger for wavenumbers and redshifts where there are cancellations in the different contributions to the total signal. The correct result is easily implemented in Zeus21.

The plan for this paper is as follows: In the next Section, we review the calculation of the correlations of components of velocities aligned with and transverse to the separation between the two points being correlated. In Section III, we describe the complete joint PDF. In Section IV we discuss the specific SFRD correlation required by Zeus21, derive the exact result, and compare it with the approximation used in Ref. [9]. We then show in Section V how our calculation impacts 21-cm observables, and we conclude in Section VI. An Appendix calculates the complete joint PDF and shows how it differs from the simple approximation adopted in Ref. [9]. A second appendix discusses the implementation in Zeus21.

II. THE VELOCITY TWO-POINT CORRELATION FUNCTION

We start with a cosmological density perturbation $\delta(\mathbf{x})$, which is assumed to be a realization of a Gaussian random field with power spectrum $P(k)$. This means that the Fourier amplitudes

$$\tilde{\delta}(\mathbf{k}) = \int d^3x e^{i\mathbf{k}\cdot\mathbf{x}} \delta(\mathbf{x}), \quad (1)$$

satisfy

$$\langle \tilde{\delta}(\mathbf{k}) \tilde{\delta}^*(\mathbf{k}') \rangle = (2\pi)^3 \delta_D(\mathbf{k} - \mathbf{k}') P(k), \quad (2)$$

where the angle brackets denote an average over all realizations, and $\delta_D(\mathbf{k} - \mathbf{k}')$ is the Dirac delta function.

At linear order, a velocity field $\mathbf{v}(\mathbf{x})$ must be $\mathbf{v}(\mathbf{x}) \propto \nabla \delta(\mathbf{x})$. For the 21-cm calculation the relevant velocity field is the baryon-dark matter relative velocity (we leave

¹ <https://github.com/JulianBMunoz/Zeus21>

out the usual subscript “bc” to reduce notational clutter). Its Fourier components $\tilde{\mathbf{v}}(\mathbf{k})$ are therefore related to those of the density field through

$$\tilde{\mathbf{v}}(\mathbf{k}) = i f(k) \mathbf{k} \tilde{\delta}(\mathbf{k}), \quad (3)$$

where $f(k)$ is a transfer function.

We now calculate the two-point correlation function for the components of the velocity field aligned with the separation between the two points at which the velocity is correlated. To do so, let us take one point as the origin and the second as the \hat{z} -axis at a distance r . Using Eqs. (1), (3), and (2), the correlation of the components aligned with the separation is then,

$$\begin{aligned} \xi_{\parallel}(r) &\equiv \langle v_z(\mathbf{0}) v_z(r\hat{z}) \rangle \\ &= \int \frac{d^3k}{(2\pi)^3} \frac{\mu^2}{k^2} e^{-ikr\mu} P(k) [f(k)]^2 \\ &= \frac{1}{4\pi^2} \int_0^\infty dk P(k) [f(k)]^2 \int_{-1}^1 d\mu \mu^2 e^{-ikr\mu} \\ &= \frac{1}{2\pi^2} \int_0^\infty dk P(k) [f(k)]^2 \left[j_0(kr) - \frac{2}{kr} j_1(kr) \right]. \end{aligned} \quad (4)$$

The correlation of the components perpendicular is

$$\begin{aligned} \xi_{\perp}(r) &\equiv \langle v_x(\mathbf{0}) v_x(r\hat{z}) \rangle \\ &= \frac{1}{2} \frac{1}{4\pi^2} \int_0^\infty dk P(k) [f(k)]^2 \int_{-1}^1 d\mu (1 - \mu^2) e^{-ikr\mu} \\ &= \frac{1}{2} \frac{1}{\pi^2} \int_0^\infty dk P(k) [f(k)]^2 \frac{j_1(kr)}{kr}, \end{aligned} \quad (5)$$

and similarly $\langle v_y(\mathbf{0}) v_y(r\hat{z}) \rangle = \xi_{\perp}(r)$. The correlation for the dot product then comes out to

$$\begin{aligned} \xi_v(r) &\equiv \langle \mathbf{v}(\mathbf{0}) \cdot \mathbf{v}(r\hat{z}) \rangle \\ &= \frac{1}{2\pi^2} \int_0^\infty dk P(k) [f(k)]^2 j_0(kr), \end{aligned} \quad (6)$$

as often seen in the literature. In these expressions, $j_n(x)$ are the spherical Bessel functions with $j_0(x) = \sin(x)/x$ and $j_1(x) = (\sin x - x \cos x)/x^2$. Fig. 1 shows the correlation coefficients $\rho_{\perp}(r) \equiv \xi_{\perp}(r)/\bar{v}^2$, $\rho_{\parallel}(r) \equiv \xi_{\parallel}(r)/\bar{v}^2$, and $\rho_v(r) \equiv \xi_v(r)/(3\bar{v}^2) = [\rho_{\parallel}(r) + 2\rho_{\perp}(r)]/3$. Here $\bar{v}^2 = \xi_{\parallel}(0) = \xi_{\perp}(0) = \xi_v(0)/3$.

III. THE JOINT PDF FOR A $\chi_{n=3}^2$ DISTRIBUTION AND FOR THE VELOCITY SQUARED

We now determine the joint PDF for the values $v_1^2 = |\mathbf{v}_1|^2$ and $v_2^2 = |\mathbf{v}_2|^2$ of the squares of the velocities \mathbf{v}_1 and \mathbf{v}_2 at two points separated by a distance r . As before, without loss of generality, we take the two points to be separated in the \hat{z} -direction. The six components (i.e.,

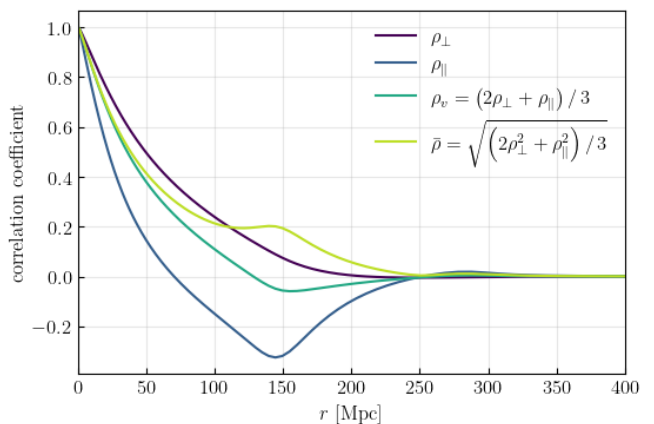


FIG. 1. The velocity correlation coefficients as functions of the separation r in units of Mpc. We show $\rho_{\parallel}(r)$ and $\rho_{\perp}(r)$ for, respectively, the components aligned with and transverse to the separation between the two points at which the velocity is correlated. We also show the isotropic correlation coefficient $\rho_v = (\rho_{\parallel}(r) + 2\rho_{\perp}(r))/3$, as well as the quantity, $[(\rho_{\parallel}^2(r) + 2\rho_{\perp}^2(r))/3]^{1/2}$ that appears in the approximation, given here in Eq. (21), of $\xi_U(r)$ in Ref.[9].

$v_{1x}, v_{1y}, v_{1z}, v_{2x}, v_{2y}, v_{2z}$) of these two velocity vectors are drawn from a Gaussian distribution with variances \bar{v}^2 . The only nonzero covariances are $\langle v_{1x} v_{2x} \rangle = \langle v_{1y} v_{2y} \rangle = \rho_{\perp} \bar{v}^2$ and $\langle v_{1z} v_{2z} \rangle = \rho_{\parallel} \bar{v}^2$.

The joint PDF for the components of \mathbf{v}_1 and \mathbf{v}_2 is then

$$P_v(\mathbf{v}_1, \mathbf{v}_2) = \frac{1}{N} \exp \left[-\frac{1}{2\bar{v}^2} \left(\frac{v_{1z}^2 + v_{2z}^2 - 2\rho_{\parallel} v_{1z} v_{2z}}{1 - \rho_{\parallel}^2} + \frac{v_{1\perp}^2 + v_{2\perp}^2 - 2\rho_{\perp} \mathbf{v}_{1\perp} \cdot \mathbf{v}_{2\perp}}{1 - \rho_{\perp}^2} \right) \right], \quad (7)$$

with

$$N = (2\pi\bar{v}^2)^3 (1 - \rho_{\parallel}^2)^{1/2} (1 - \rho_{\perp}^2). \quad (8)$$

The joint PDF for $X_1 \equiv v_1^2$ and $X_2 \equiv v_2^2$, is then

$$P(X_1, X_2) = \int d^3v_1 \int d^3v_2 P_v(\mathbf{v}_1, \mathbf{v}_2) \times \delta_D(X_1 - v_1^2) \delta_D(X_2 - v_2^2). \quad (9)$$

Section A shows how this is evaluated and related in the limit $\rho_{\perp} \rightarrow \rho_{\parallel}$ to the expression used in Ref. [9]. However, we will now see that Eq. (9) is a good starting point for the required calculation.

For reference, Ref. [9] approximates this joint PDF with Eq. (9) but using a joint velocity PDF where ρ_{\perp} and ρ_{\parallel} are both taken to be $\bar{\rho}$.

IV. IMPLICATIONS FOR 21-CM CALCULATION

We now show how these PDFs enter into Zeus21. The correlations required there are for exponential fields,

$e^{\lambda_\alpha Y(\mathbf{x})}$, where $Y = v^2(\mathbf{x})/\bar{v}^2$, and λ_α is a coefficient that depends on the specific quantity (e.g., stellar density, star formation rate, etc.). Most generally, the correlation will be a cross-correlation between two populations labeled by $\alpha = 1$ and $\alpha = 2$, in which case we need cross-correlation functions for the quantities $U_1 = e^{-\lambda_1 Y_1(\mathbf{x}_1)}$ and $U_2 = e^{-\lambda_2 Y_2(\mathbf{x}_2)}$ at two different points separated by a comoving distance $r = |\mathbf{x}_1 - \mathbf{x}_2|$. (Note that our Y_α is referred to as $\tilde{\eta}_\alpha$ in Ref. [9], and our \bar{v}^2 is σ^2 there.)

The correlation function for Y is

$$\xi_Y(r) \equiv \frac{\langle Y(\mathbf{x}_1)Y(\mathbf{x}_2) \rangle - \langle Y \rangle^2}{\langle Y \rangle^2} = \frac{2\rho_{\parallel}^2 + 4\rho_{\perp}^2}{9}. \quad (10)$$

The required two-point correlation for U_α is then

$$\xi_U(r) = \frac{\langle U_1 U_2 \rangle - \langle U_1 \rangle \langle U_2 \rangle}{\langle U_1 \rangle \langle U_2 \rangle}. \quad (11)$$

The expectation values of U_α are

$$\langle U_\alpha \rangle \equiv (1 + 2\lambda_\alpha)^{-3/2}, \quad (12)$$

while that for the product is

$$\langle U_1 U_2 \rangle \equiv \iiint U_1 U_2 P(Y_1, Y_2) dY_1 dY_2 \quad (13)$$

$$= \iiint e^{-(\lambda_1 Y_1 + \lambda_2 Y_2)} P(Y_1, Y_2) dY_1 dY_2. \quad (14)$$

Given the Dirac delta functions in Eq. (9), this becomes

$$\langle U_1 U_2 \rangle = \int d^3 v_1 \int d^3 v_2 e^{-\lambda_1 Y_1 - \lambda_2 Y_2} P_v(\mathbf{v}_1, \mathbf{v}_2). \quad (15)$$

The six integrals can now be separated as $\langle U_1 U_2 \rangle = I_{\parallel} I_{\perp}^2$, with

$$I_{\parallel} = \int dv_1 dv_2 e^{-(\lambda_1 v_1^2 + \lambda_2 v_2^2)/\bar{v}^2} P_{\parallel}(v_1, v_2), \quad (16)$$

and

$$P_{\parallel}(v_1, v_2) = \frac{1}{2\pi\bar{v}^2} \exp \left[-\frac{1}{2\bar{v}^2} \left(\frac{v_1^2 + v_2^2 - 2\rho_{\parallel} v_1 v_2}{1 - \rho_{\parallel}^2} \right) \right]. \quad (17)$$

Eq. (16) then evaluates to

$$I_{\parallel} = \left[1 + 2\lambda_1 + 2\lambda_2 + 4\lambda_1 \lambda_2 (1 - \rho_{\parallel}^2) \right]^{-1/2}. \quad (18)$$

The result for I_{\perp} is the same with $\parallel \rightarrow \perp$.

Putting it all together, Eq. (11) becomes

$$\xi_U = \left[\left(1 - K\rho_{\parallel}^2 \right) \left(1 - K\rho_{\perp}^2 \right) \right]^{-1/2} - 1, \quad (19)$$

where

$$K \equiv \frac{4\lambda_1 \lambda_2}{(1 + 2\lambda_1)(1 + 2\lambda_2)}. \quad (20)$$

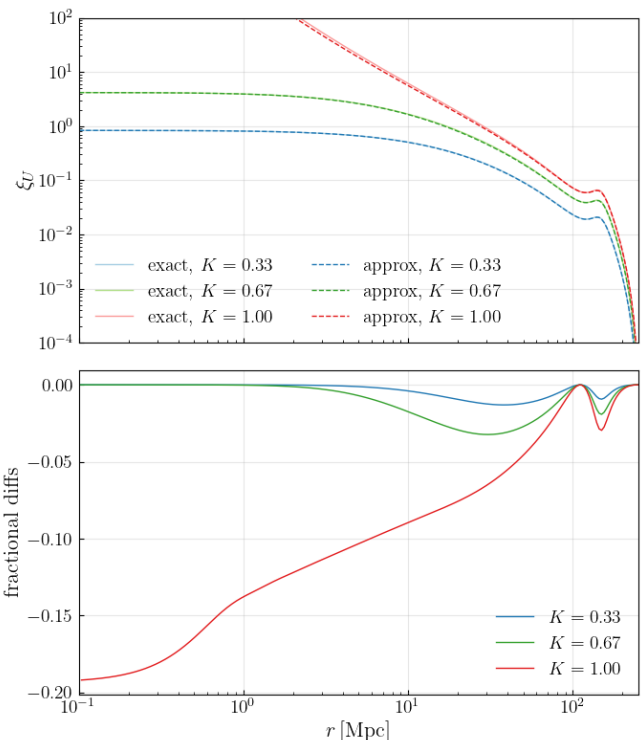


FIG. 2. Here we show $\xi_U(r)$ from the exact and approximate calculations, using the velocity correlation functions in Fig. 1 for values of $K = 0.33, 0.67$, and 1 . The values of K required for 21-cm fluctuations are typically around $K \simeq 0.5$.

The new result in Eq. (19) is to be contrasted with that [9]

$$\xi_U = \left[1 - K(\rho_{\parallel}^2 + 2\rho_{\perp}^2)/3 \right]^{-3/2} - 1, \quad (21)$$

obtained under the assumption that all three components of the peculiar velocity have the same correlation coefficient ρ . Written in this way, it is clear that the new result in Eq. (19) reduces to the result of Ref. [9] in the limit $\rho_{\perp}^2 \rightarrow \rho_{\parallel}^2$. However, in general it differs.

Most generally, $0 < K < 1$, but typical values of λ_α for the 21-cm calculation are $\simeq 1$, implying $K \simeq 0.5$ typically. The correlations die off at large distances, and so as $r \rightarrow \infty$, $K\rho_{\perp}^2, K\rho_{\parallel}^2 \ll 1$, and the correct correlation function becomes $\xi_U \simeq K(\rho_{\parallel}^2 + 2\rho_{\perp}^2)/2$ and, in this limit, coincides with the approximation. The correction is expected to be larger at smaller r , where $\rho_{\parallel}(r)$ and $\rho_{\perp}(r)$ become larger, but this is then counteracted by the fact that both approach unity as $r \rightarrow 0$. Fig. 2 shows results for the fractional difference in $\xi_U(r)$ for several values of K .

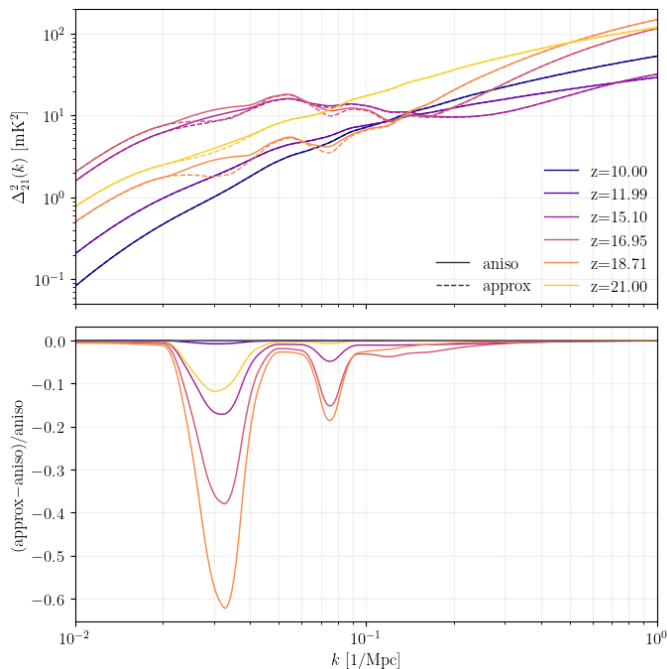


FIG. 3. The top panel shows the 21-cm intensity-fluctuation power spectrum $\Delta_{21}^2(k)$ for several redshifts. The solid curves are the **Zeus21** calculation, while the dashed are obtained by modifying **Zeus21** to include the correct squared-velocity PDFs. The calculations include Pop III stars and baryon-dark matter relative velocities with the parameters used in the **Zeus21** tutorial. The correction is very small for most wavenumbers k and redshifts z , but becomes large for a limited range of wavenumbers at redshifts $z \simeq 15$ when there are cancellations between the different contributions to the total signal.

V. EFFECTS OF THE ANISOTROPY ON THE 21-CM POWER SPECTRUM

The correlation function $\xi_U(r)$ enters into expressions for correlation functions of SFRDs, which then contribute to 21-cm fluctuations. However, these are not the whole story; there are other sources of 21-cm fluctuations. Thus, to assess the impact of the exact PDF calculation, we run **Zeus21** using the exact and approximate expressions for $\xi_U(r)$. The top panel of Fig. 3 shows the 21-cm power spectra $\Delta_{21}^2(k)$ as a function of

wavenumber k for several redshifts z for the isotropic assumption in **Zeus21** (solid curve) and the calculation described here (dashed). The bottom panel shows the fractional differences between the approximate and exact calculation. The differences are no more than a few percent for most wavenumbers and redshifts, but get larger for a limited range of k at redshifts $z \simeq 15$ where there are cancellations between different contributions to the total signal. These calculations were performed for the default parameters in **Zeus21**. We note the precise magnitude of the correction, as well as the wavenumbers and redshifts where cancellations may occur, may be highly model dependent.

VI. CONCLUSIONS

To conclude, we have discussed a subtlety in the calculation of the PDF of the squares of the peculiar velocity and investigated the implications for 21-cm fluctuations. While the error introduced by overlooking this effect is generally small compared with other current sources of uncertainty, it may become big for wavenumbers and redshifts where there are cancellations between different contributions to the total signal. It is easily implemented (as we detail in Section B below) in the existing code and may become important in the future as we seek to interpret increasingly precise measurements.

ACKNOWLEDGMENTS

We thank Hector Cruz for discussions. RYZ acknowledges the support of a Johns Hopkins University Summer Provost's Undergraduate Research Award. This work was supported by NSF Grant No. 2412361, NASA ATP Grant No. 80NSSC24K1226, and the Templeton Foundation.

Appendix A: The full joint PDF

We evaluate the full joint PDF by writing \mathbf{v}_1 and \mathbf{v}_2 in Eq. (9) in spherical coordinates taking, without loss of generality v_1 to lie in the xz -plane, with azimuthal coordinate $\phi = 0$. The joint PDF then becomes,

$$\begin{aligned}
 P(X_1, X_2) = & \frac{\pi}{N} \exp \left[-\frac{X_1 + X_2}{2\bar{v}^2(1 - \rho_{\perp}^2)} \right] \int_{-\sqrt{X_1}}^{\sqrt{X_1}} dv_{1z} \int_{-\sqrt{X_2}}^{\sqrt{X_2}} dv_{2z} I_0 \left(\frac{\rho_{\perp} \sqrt{X_1 - v_{1z}^2} \sqrt{X_2 - v_{2z}^2}}{(1 - \rho_{\perp}^2) \bar{v}^2} \right) \\
 & \times \exp \left[-\frac{1}{2\bar{v}^2} \left(\frac{\rho_{\parallel}^2 - \rho_{\perp}^2}{(1 - \rho_{\parallel}^2)(1 - \rho_{\perp}^2)} (v_{1z}^2 + v_{2z}^2) - \frac{2\rho_{\parallel}}{1 - \rho_{\parallel}^2} v_{1z}v_{2z} \right) \right], \quad (\text{A1})
 \end{aligned}$$

where $I_0(x)$ is a modified Bessel function of the first kind,

and N is given in Eq. (8).

In the limit that $\rho_{\perp} \rightarrow \rho_{\parallel} \equiv \rho$, this becomes equivalent to the results in Refs. [6, 9]; i.e.,

$$P_{\text{sym}}(X_1, X_2) = \frac{(1 - \rho^2)^{3/2} (X_1 X_2)^{1/2}}{4\pi} \exp\left(-\frac{X_1 + X_2}{2(1 - \rho^2)}\right) \times \int_{-1}^1 \exp\left(\mu \frac{\rho \sqrt{X_1 X_2}}{(1 - \rho^2)}\right). \quad (\text{A2})$$

Appendix B: Changes to Zeus21

The implementation of the corrected PDFs in Zeus21 is straightforward. A few changes are required in `cosmology.py` and then more in `correlations.py`. The calculation of $P_{\eta}(k)$ in `cosmology.py` must be replaced by calculations of $P_{\eta,\perp}(k)$ and $P_{\eta,\parallel}(k)$. To get the for-

mer, the factor $6\psi_0^2 + 3\psi_2^2$ in the expression for $P_{\eta}(k)$ is replaced by $6(\psi_0 - \psi_2/2)^2$ and the latter is obtained by replacing that factor with $6(\psi_0 + \psi_2)^2$.

The quantity `xiNumerator` in the function `get_xi_Sum_2expEta` in `correlations.py` must then be altered so that the four evaluations of ξ_U are corrected. There are several steps in `correlations.py` intermediate between the evaluation of $P_{\eta}(k)$ in `cosmology.py` and its appearance in `xiNumerator` that must be modified to replace $P_{\eta}(k)$ with $P_{\eta,\parallel}(k)$ and $P_{\eta,\perp}(k)$.

These modifications require two evaluations of `mcfits` (which transforms between correlation functions and power spectra) to obtain $P_{\eta,\perp}(k)$ and $P_{\eta,\parallel}(k)$, rather than one for $P_{\eta}(k)$, but the increase to the total runtime is only a few percent.

-
- [1] J. B. Muñoz, Standard Ruler at Cosmic Dawn, *Phys. Rev. Lett.* **123**, 131301 (2019), arXiv:1904.07868 [astro-ph.CO].
 - [2] J. B. Muñoz, Robust Velocity-induced Acoustic Oscillations at Cosmic Dawn, *Phys. Rev. D* **100**, 063538 (2019), arXiv:1904.07881 [astro-ph.CO].
 - [3] K. M. Smith and S. Ferraro, Detecting Patchy Reionization in the Cosmic Microwave Background, *Phys. Rev. Lett.* **119**, 021301 (2017), arXiv:1607.01769 [astro-ph.CO].
 - [4] N. Anil Kumar, M. Çalıřkan, S. C. Hotinli, M. Kamionkowski, S. Ferraro, and K. Smith, Patchy Helium and Hydrogen Reionization from the Kinetic Sunyaev-Zel'dovich Effect and Galaxies, (2025), arXiv:2506.11188 [astro-ph.CO].
 - [5] N. Anil Kumar, M. Çalıřkan, S. C. Hotinli, K. Smith, and M. Kamionkowski, Electrons Everywhere, All at Once: A Novel kSZ Estimator for Electron-Electron Correlations, (2025), arXiv:2509.18249 [astro-ph.CO].
 - [6] J. J. Givans and M. Kamionkowski, Hints of tensions in the cosmic microwave background temperature and polarization quadrupoles, (2023), arXiv:2311.06196 [astro-ph.CO].
 - [7] W. J. Percival and M. L. Brown, Likelihood methods for the combined analysis of CMB temperature and polarization power spectra, *Mon. Not. Roy. Astron. Soc.* **372**, 1104 (2006), arXiv:astro-ph/0604547.
 - [8] S. Hamimeche and A. Lewis, Likelihood Analysis of CMB Temperature and Polarization Power Spectra, *Phys. Rev. D* **77**, 103013 (2008), arXiv:0801.0554 [astro-ph].
 - [9] H. A. G. Cruz, J. B. Munoz, N. Sabti, and M. Kamionkowski, Effective model for the 21-cm signal with population III stars, *Phys. Rev. D* **111**, 083503 (2025), arXiv:2407.18294 [astro-ph.CO].